Available online at www.sciencedirect.com
ScienceDirect
Journal of Sound and Vibration 304 (2007) 72–90
JOURNAL OF SOUND AND VIBRATION
www.elsevier.com/locate/jsvi

Dynamic response of arch bridges traversed by high-speed trains

Walter Lacarbonara[a,*], Valerio Colone[b,1]

[a]Dipartimento di Ingegneria Strutturale e Geotecnica, Sapienza Università di Roma, via Eudossiana 18, 00184 Rome, Italy
[b]Dipartimento di Scienze dell'Ingegneria Civile, Università Roma Tre, via Vito Volterra 62, 00146 Rome, Italy

Received 17 October 2005; received in revised form 15 January 2007; accepted 30 January 2007

Abstract

A mechanical model describing the planar elasto-dynamics of arch bridges with general arch profiles is presented. The model is amenable to analytical or semi-analytical treatments and is effective for parametric studies, design of control systems or structural optimizations. The Ritz's energy approach is employed to calculate the solutions of the vibration eigenvalue problem—natural frequencies and mode shapes—and the forced responses to external excitations, namely those induced by the passage of trains. A closed-form solution of the bridge dynamic response to the transit of trains with arbitrary load distributions and running speeds is found and the train-induced resonances are accordingly discussed. In particular, three European high-speed trains—the French TGV, the Italian ETR 500, and the German ICE—traversing a lower-deck steel arch bridge are considered and the ensuing responses are investigated.

1. Introduction

The dynamic response of bridges traversed by trains is a subject of interest in structural engineering due to the increasing train speeds which will become significantly higher with the next-generation magnetically levitated trains. From a structural point of view and the passenger comfort, the noise disturbance and bridge vibrations cause undesirable effects that need to be dealt with and become more serious during the train acceleration phases.

Early studies considered the bridge as a simply supported beam and the train as a moving load with constant speed. Later, Bolotin [1] studied a beam subject to an infinite sequence of equal loads uniformly spaced by a distance d and moving at constant speed $\bar{V}$. In his study, the period of the moving loads, $d/\bar{V}$, was identified as the key parameter. Along the same lines, Fryba [2] concluded that the forced steady-state vibratory response will attain its maximum when the time interval between two successive loads is equal to or is an integer multiple of some natural periods of the beam in free oscillations. Besides straight beams, also the dynamic response of circular arches subject to a concentrated load moving along the circumferential direction has been recently studied in Ref. [3].

A few investigations [4] have considered the nonlinear resonances that can be excited by a single load traversing a bridge, modelled as an Euler–Bernoulli beam resting on nonlinear visco-elastic supports, and have

*Corresponding author. Tel.: +39 6 44 585 293; fax: +36 6 488 4852.
E-mail address: walter.lacarbonara@uniroma1.it (W. Lacarbonara).
[1]Currently, Engineer, Technip Italy, 68 Viale Castello della Magliana, 00148 Rome, Italy.

0022-460X/$ - see front matter © 2007 Elsevier Ltd. All rights reserved.
doi:10.1016/j.jsv.2007.01.037

shown that, in addition to the primary resonances of the bending modes, when the forcing levels are high there are many secondary resonances exciting responses that can be significantly more complex compared with those exhibited by the linear model.

Recent studies have investigated the dynamic behaviour of railway bridges employing detailed models of the bridges and passing trains. For example, Au et al. [5] used five models of moving vehicles to study the impact effects on a cable-stayed bridge under railway train loading. The rail irregularities and the geometric nonlinear behaviour of the cable-stayed bridge were taken into account.

Yang et al. [6] presented a closed-form solution of the dynamic response of simply supported Euler–Bernoulli beams subjected to the passage of high-speed trains where the phenomena of resonance and cancellation were identified, along with optimal design criteria. Klasztorny [7] presented an iterative algorithm for solving vertical vibrations of a multi-span steel bridge, induced by a fast passenger train, moving at a speed of 120–360 km/h. Xia and Zhang [8] studied the dynamic interaction between a high-speed train and the bridge by theoretical analysis and field experiments. Each vehicle was described by 27 degrees of freedom whereas the bridge was modelled by the modal superposition technique. They showed a good agreement between the calculated results and the in situ measured data.

In recent years, the dynamic behaviour of high-speed railway bridges has been extensively investigated mainly via field tests aimed at improving the design of high-speed railways. Xia et al. [9] reported the experimental results—deflections, accelerations, strains—relating to a prestressed concrete bridge, the Gouhe River Bridge, traversed by the China-Star high-speed train (design speed of 270 km/h) that reached the peak speed of about 320 km/h. Kwark et al. [10] conducted experimental and theoretical studies to determine the dynamic behaviour of bridges crossed by the Korean high-speed train (KHST). For running speeds close to the critical speed (i.e., the train speed at which one of the bridge modes is excited), greatly amplified dynamic responses compared with the static responses were observed. They adopted three-dimensional (3D) models to represent the dynamic interaction between the articulated bogies train and the bridge and showed reasonable agreements.

Most of the referenced theoretical and experimental investigations relate to simply supported single- or multi-span straight bridges. Nonetheless, steel or prestressed concrete arch bridges are typical structural schemes in the medium-/long-span bridge category, normally constructed in mountain areas. A good number of works dealt with 2D elastic and inelastic modelling of upper-deck steel arch bridges to investigate the in-plane bridge responses to earthquakes (see, e.g., Ref. [11]). Only a few studies have considered the dynamic behaviour of lower-deck arch bridges under train loads. In Ref. [12], the vibration characteristics of steel arch bridges traversed by high-speed trains were investigated. Two simple criteria were determined to predict the train–bridge resonance effects and validated the predictions employing finite element (FE) analyses.

In the present work, the dynamic response of arch bridges is investigated employing a mechanical parametric model, based on pertinent kinematic assumptions, and suitable to describe the structural elasto-dynamic responses to general planar excitations and, in particular, to the passage of trains. The distributed-parameter (DP) model allows efficient parametric studies as well as the effective design of vibration control schemes aimed at improving the structural integrity and passenger comfort which is the main focus of an accompanying paper. Employing the proposed mechanical model, the elasto-dynamic responses to the passage of arbitrary trains are obtained in closed form along with the train-induced primary resonances of arbitrary bridge modes.

In Section 2, the arch bridge analytical model is presented. In Section 3, the semi-analytical computational strategy is discussed. In Section 4, the closed-form bridge response to the passage of an arbitrary train is shown; the resonance speeds are discussed in Section 5. In Section 6, the main results relating to a steel arch bridge traversed by three European high-speed trains are reported. In Section 7, the main conclusions are drawn.

2. Equations of motion for arch bridges

In this section, the DP model describing planar elasto-dynamic responses of arch bridges with general arch profiles of the lower- or upper-deck type is illustrated. To the best of the author's knowledge, this approach has not been employed in former studies on arch bridge dynamics. The model (see Fig. 1a) comprises three

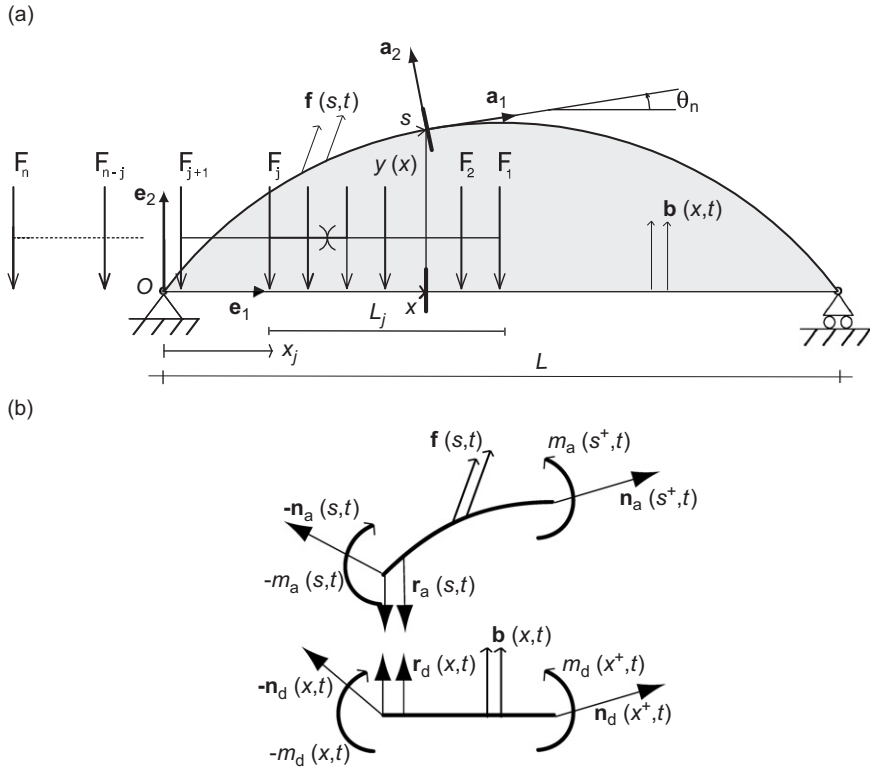

Fig. 1. (a) Schematic description of the arch bridge model with the train loading and (b) free-body diagram of the internal and external forces.

elements, namely, the arch, the horizontal beam (i.e., the bridge deck), and the vertical hanger rods connecting the arch to the deck. The following assumptions are adopted: (i) the hanger rods are hinged at both ends and, due to their high axial stiffness, they are assumed inextensible; (ii) the spacing between the hanger rods is small enough compared with the bridge span L so that an equivalent continuous distribution of hanger elements is considered; (iii) the bridge possesses a plane of symmetry coinciding with the plane where the external load resultants lie and the bridge motions occur. The latter assumption justifies a planar model. Out-of-plane vibrations (i.e., out-of-plane flexural and torsional motions) are neglected because the passage of trains on single-track bridges as the one here considered and the earthquakes generate prevalently in-plane forces. The hypothesis of inextensibility of the hanger rods is based on previous studies which have shown that the relatively small axial flexibility of the hanger rods does not introduce appreciable effects in the global responses. For example, in the context of suspension footbridges, Brownjohn [13,14] employed a continuum model based on inextensible connections between the deck and the suspension cables and showed a good agreement between the theoretically obtained and experimentally measured natural frequencies.

In Fig. 1a, $(O, \mathbf{e}_1, \mathbf{e}_2, \mathbf{e}_3)$ represents a fixed inertial reference frame whereas $(\mathbf{a}_1, \mathbf{a}_2, \mathbf{a}_3)$ is an orthonormal local frame for the arch with $\mathbf{a}_1$ tangent to the undeformed arch centroidal line. The coordinate x along the fixed $\mathbf{e}_1$-direction (centreline of the undeformed deck) is chosen as the independent space coordinate. Consequently, the elasto-dynamic problem is parameterized with $x \in [0, L]$ and time $t \in [0, \infty)$. The arclength parameter s along the arch undeformed centroidal line is used only as an intermediate variable as it allows to express naturally the arch strains as well as the arch balance laws. The choice of the horizontal coordinate x as the independent coordinate is justified by the fact that the distribution of the loads (the trains run on the rail tracks fixed onto the deck) is more simply expressed in this coordinate.

The arch kinematic descriptors are the displacement vector, $\mathbf{u}(x,t) = u(x,t)\mathbf{e}_1 + v(x,t)\mathbf{e}_2$, representing the displaced position of the centroidal line of the arch, and the rotation angle of the arch cross-section, $\boldsymbol{\theta}_a(x,t) = \theta_a(x,t)\,\mathbf{e}_3$. The displacement components u and v represent the horizontal and vertical displacements

of the arch centreline, respectively. Due to the kinematic constraint represented by the inextensible hanger rods, the vertical displacement of the horizontal beam is the same as the arch vertical displacement, $v(x,t)$. This motivates the use of the arch displacement components in the $(\mathbf{e}_1,\mathbf{e}_2)$-basis rather than the local displacement components in the intrinsic $(\mathbf{a}_1,\mathbf{a}_2)$-basis, namely the tangential and radial displacements.

Longitudinal forces on the deck are neglected; therefore, the longitudinal motion of the deck is not considered. Further, since the bridge deck, due to its slenderness, is modelled as an Euler–Bernoulli beam, the rotation of its cross-section is related to the vertical displacement as $\boldsymbol{\theta}_d = (\partial v/\partial x)\mathbf{e}_3$.

The linearized arch strain vector is $\boldsymbol{\varepsilon}_a = \partial\mathbf{u}/\partial s - \boldsymbol{\theta}_a \times \mathbf{a}_1$, where $\times$ denotes the vector product. The components of the arch strain vector in the local basis, $\boldsymbol{\varepsilon}_a = \varepsilon_a\mathbf{a}_1 + \eta_a\mathbf{a}_2$, are the elongation ε_a and shear strain η_a, respectively, and are expressed in terms of the horizontal coordinate as

$$\varepsilon_a = \frac{\partial u}{\partial x}\cos^2\theta_n + \frac{1}{2}\frac{\partial v}{\partial x}\sin 2\theta_n, \quad \eta_a = -\frac{1}{2}\frac{\partial u}{\partial x}\sin 2\theta_n + \frac{\partial v}{\partial x}\cos^2\theta_n - \theta_a, \tag{1}$$

where θ_n is the angle between the tangent to the arch undeformed centreline and the horizontal line. Use of the following identities has been made: $\partial/\partial s = (\mathrm{d}x/\mathrm{d}s)(\partial/\partial x) = \cos\theta_n(\partial/\partial x)$, $\cos\theta_n = \mathbf{a}_1\cdot\mathbf{e}_1$, $\mathbf{a}_1\cdot\mathbf{e}_2 = \sin\theta_n$, $\mathbf{a}_2\cdot\mathbf{e}_1 = -\sin\theta_n$, $\mathbf{a}_2\cdot\mathbf{e}_2 = \cos\theta_n$, where the dot indicates the standard inner product in Euclidean space. When the arch profile is described by the function $y(x)$, then $\theta_n = \arctan(y')$, $\cos\theta_n = (\sqrt{1+y'^2})^{-1}$, and $\sin\theta_n = y'(\sqrt{1+y'^2})^{-1}$, where the prime denotes differentiation with respect to x.

The arch bending curvature is $\kappa_a = \partial\theta_a/\partial s = \partial\theta_a/\partial x\cos\theta_n$, whereas the bending curvature of the unshearable deck is $\kappa_d = \partial\theta_d/\partial x = \partial^2 v/\partial x^2$. The subscripts a and d, here and henceforth, will denote the arch and the deck, respectively.

Since also the arch is slender, the arch shear strain is neglected as well imposing the internal kinematic constraint $\eta_a \equiv 0$. This constraint yields the arch section rotation field and, hence, the arch bending curvature as

$$\theta_a = -\frac{1}{2}\frac{\partial u}{\partial x}\sin 2\theta_n + \frac{\partial v}{\partial x}\cos^2\theta_n, \quad \kappa_a = \cos\theta_n\frac{\partial}{\partial x}\left(-\frac{1}{2}\frac{\partial u}{\partial x}\sin 2\theta_n + \frac{\partial v}{\partial x}\cos^2\theta_n\right). \tag{2}$$

Therefore, the non-zero strains describing the arch bridge planar deformation processes are the arch elongation ε_a and its bending curvature κ_a, and the deck bending curvature κ_d. The unknown functions are the displacement components $u(x,t)$ and $v(x,t)$. Accounting for the elasticity of the hanger rods would increase the number of unknowns from two to three or four since, in the latter case, the arch motions and the deck motions would be independent. However, previous studies have shown that the relatively small axial flexibility of the hanger rods does not introduce appreciable effects onto the arch bridge global responses.

A free-body diagram, with the internal and external forces, is shown in Fig. 1b. Let the internal contact forces and couples, mutually exerted by two adjoining sections, in the arch and the deck be expressed, respectively, as

$$\begin{aligned} &\mathbf{n}_a(x,t) = N_a\mathbf{a}_1 + H_a\mathbf{a}_2, \quad \mathbf{m}_a(x,t) = M_a(x,t)\mathbf{a}_3,\\ &\mathbf{n}_d(x,t) = H_d\mathbf{e}_2, \quad \mathbf{m}_d(x,t) = M_d(x,t)\mathbf{e}_3, \end{aligned} \tag{3}$$

where N_j and H_j $(j = a,d)$ indicate the axial load and shear force, respectively, and M_j is the bending moment. Moreover, let the hanger-rod reactive force per unit reference length s acting on the arch be $\mathbf{r}_a$ and the reactive force per unit reference length x acting on the deck be $\mathbf{r}_d$. They are expressed as $\mathbf{r}_a = -r\cos\theta_n\mathbf{e}_2$ and $\mathbf{r}_d = r\mathbf{e}_2$ where $r(x)$ denotes the magnitude of the force per unit reference length x.

The balance of linear momentum and angular momentum, in the undeformed configurations of the arch and the deck, are expressed, respectively, in the form

$$\frac{\partial\mathbf{n}_a}{\partial s} + \mathbf{r}_a + \mathbf{f} = (\rho A)_a\frac{\partial^2\mathbf{u}}{\partial t^2}, \quad \frac{\partial M_a}{\partial s} + H_a = 0, \tag{4}$$

$$\frac{\partial\mathbf{n}_d}{\partial x} + \mathbf{r}_d + \mathbf{b} = (\rho A)_d\frac{\partial^2 v}{\partial t^2}\mathbf{e}_2, \quad \frac{\partial M_d}{\partial x} + H_d = 0, \tag{5}$$

where $\mathbf{f} = f_1\mathbf{e}_1 + f_2\mathbf{e}_2$ is the force per unit reference length s acting on the arch and $\mathbf{b} = b\mathbf{e}_2$ is the force per unit reference length x acting on the deck, respectively; $(\rho A)_a$ and $(\rho A)_d$ are the masses per unit reference length

along the arch and the deck, respectively. Once the reactive shear forces H_a and H_d are eliminated from the equations using $H_a = -\partial M_a/\partial s$ and $H_d = -\partial M_d/\partial x$, the resulting balance laws are put in componential form, in the $(\mathbf{e}_1, \mathbf{e}_2)$-basis, as

$$\left(\frac{\partial N_a}{\partial s} + k_n \frac{\partial M_a}{\partial s}\right) \cos\,\theta_n - \left(k_n N_a - \frac{\partial^2 M_a}{\partial s^2}\right) \sin\theta_n + f_1 = (\rho A)_a \frac{\partial^2 u}{\partial t^2}, \tag{6}$$

$$\left(\frac{\partial N_a}{\partial s} + k_n \frac{\partial M_a}{\partial s}\right) \sin\theta_n + \left(k_n N_a - \frac{\partial^2 M_a}{\partial s^2}\right) \cos\theta_n - r\cos\theta_n + f_2 = (\rho A)_a \frac{\partial^2 v}{\partial t^2}, \tag{7}$$

$$-\frac{\partial^2 M_d}{\partial x^2} + r + b = (\rho A)_d \frac{\partial^2 v}{\partial t^2}. \tag{8}$$

where $k_n = \mathrm{d}\theta_n/\mathrm{d}s$ is the geometric curvature of the undeformed arch. Dividing Eqs. (6) and (7) by $\cos\,\theta_n$ (different from zero $\forall\, x \in [0, L]$) solving Eq. (8) for the hanger internal force density r, substituting the result into the previous two equations, and considering the change of coordinate from s to x yield the following two governing equations of motion:

$$(\rho A)_a \sec\,\theta_n \frac{\partial^2 u}{\partial t^2} - \frac{\partial}{\partial x}(N_a\,\cos\theta_n) - \frac{1}{2}\frac{\partial}{\partial x}\left(\frac{\partial M_a}{\partial x}\sin 2\theta_n\right) = f_1\,\sec\,\theta_n, \tag{9}$$

$$[(\rho A)_d + (\rho A)_a \sec\theta_n]\frac{\partial^2 v}{\partial t^2} - \frac{\partial}{\partial x}(N_a \sin\theta_n) + \frac{\partial}{\partial x}\left(\frac{\partial M_a}{\partial x}\cos^2\theta_n\right) + \frac{\partial^2 M_d}{\partial x^2} = f_2\,\sec\,\theta_n + b. \tag{10}$$

Equation (10), representing the balance equation in the vertical direction, besides the bending load-carrying term due to the horizontal deck, M_d'', comprises two load-carrying terms delivered by the arch, namely that arising from the arch axial load $(N_a\,\sin\theta_n)'$, and the arch flexural term, $(M_a'\cos^2\theta_n)'$. The relative magnitude of the funicular term with respect to the arch flexural term depends on the distributions of the loads acting on the bridge and the arch. Clearly, neglecting these two load-carrying terms along with the arch inertia yields the equation of motion of a single-span simply supported bridge.

Because a linearized model is being considered (the strains and displacements are assumed infinitesimally small), linear elastic constitutive laws relating the internal forces to the strains are adopted in the standard form

$$N_a = (EA)_a \varepsilon_a = (EA)_a \left[\frac{\partial u}{\partial x}\cos^2\theta_n + \frac{1}{2}\frac{\partial v}{\partial x}\,\sin\,2\theta_n\right], \tag{11}$$

$$M_a = (EJ)_a \kappa_a = (EJ)_a \left[\frac{\partial}{\partial x}\left(-\frac{1}{2}\frac{\partial u}{\partial x}\,\sin 2\theta_n + \frac{\partial v}{\partial x}\cos^2\theta_n\right)\cos\,\theta_n\right], \tag{12}$$

$$M_d = (EJ)_d \kappa_d = (EJ)_d \frac{\partial^2 v}{\partial x^2}, \tag{13}$$

where $(EA)_a$ and $(EJ)_a$ are the axial and bending stiffnesses of the arch, respectively; $(EJ)_d$ is the bending stiffness of the bridge deck.

Assuming uniform arch and deck properties, the following non-dimensional variables and parameters are introduced:

$$x^* = \frac{x}{L}, \quad u^* = \frac{u}{L}, \quad v^* = \frac{v}{L}, \quad t^* = \omega_a t,$$

$$\omega_a = \sqrt{\frac{(EJ)_a}{(\rho A)_a L^4}}, \quad \mu = \frac{(\rho A)_d}{(\rho A)_a}, \quad \alpha = \frac{(EA)_a}{(EJ)_a}L^2, \quad \gamma = \frac{(EJ)_d}{(EJ)_a},$$

$$p_1 = \frac{f_1}{(EJ)_a} L^3, \quad p_2 = \frac{f_2}{(EJ)_a} L^3, \quad q = \frac{b}{(EJ)_a} L^3.$$

Omitting the star, for notational simplicity, the non-dimensional arch bridge equations of motion can be expressed as

$$\sec\theta_n \frac{\partial^2 u}{\partial t^2} - \alpha \frac{\partial}{\partial x}\left[\left(\frac{\partial u}{\partial x}\cos^2\theta_n + \frac{1}{2}\frac{\partial v}{\partial x}\sin 2\theta_n\right)\cos\theta_n\right] - \frac{1}{2}\frac{\partial}{\partial x}\left\{\sin 2\theta_n \frac{\partial}{\partial x}\left[\frac{\partial}{\partial x}\left(-\frac{1}{2}\frac{\partial u}{\partial x}\sin 2\theta_n + \frac{\partial v}{\partial x}\cos^2\theta_n\right)\cos\theta_n\right]\right\} = p_1(x,t)\sec\theta_n, \tag{14}$$

$$(\mu + \sec\theta_n)\frac{\partial^2 v}{\partial t^2} - \alpha \frac{\partial}{\partial x}\left[\left(\frac{\partial u}{\partial x}\cos^2\theta_n + \frac{1}{2}\frac{\partial v}{\partial x}\sin 2\theta_n\right)\sin\theta_n\right] + \frac{\partial}{\partial x}\left\{\cos^2\theta_n \frac{\partial}{\partial x}\left[\frac{\partial}{\partial x}\left(-\frac{1}{2}\frac{\partial u}{\partial x}\sin 2\theta_n + \frac{\partial v}{\partial x}\cos^2\theta_n\right)\cos\theta_n\right]\right\} + \gamma\frac{\partial^4 v}{\partial x^4} = p_2(x,t)\sec\theta_n + q(x,t). \tag{15}$$

Equations (14) and (15) are supplemented with the pertinent boundary conditions.

3. Semi-analytical solution strategy and model validation

The equations of motion (14) and (15) are linear partial-differential equations with variable coefficients due to the non-uniform geometric curvature of the arch profile. Closed-form solutions cannot be found for general arch profiles and loading conditions. However, semi-analytical methods can be effectively employed to make the subsequent studies more efficient allowing also a closed-form representation of the solution, especially in view of the investigations into general signatures of the elasto-dynamic responses and the design of tuned-mass damper systems for vibration mitigation which will be discussed in a companion paper. Viable semi-analytical strategies are the method of weighted residuals in the form due to Galerkin (where the balance laws (14) and (15) are directly used to minimize the residual forces over the domain once the unknown displacement is expressed in terms of admissible functions) or the energy approach due to Ritz.

For the considered self-adjoint problem, the two approaches, although differing in the computational implementations, yield the same set of algebraic equations. However, the Ritz's method can be more easily implemented resorting to the bridge energy functionals. The discretizing functions are to be chosen from a complete set of admissible functions satisfying the geometric boundary conditions. Here, they are chosen within the set of comparison functions satisfying both the geometric and mechanical boundary conditions. Considering the case of simply supported boundary conditions, the unknown displacement components u and v are then expressed as

$$u(x,t) = \sum_{j=1}^{N_u}\{\xi_j(t)\sin(j\pi x) + j\zeta_j(t)y_j(x)\}, \quad v(x,t) = \sum_{j=1}^{N_v}\zeta_j(t)\sin(j\pi x), \tag{16}$$

where $\xi_j(t)$ and $\zeta_j(t)$ are the generalized coordinates, $(N_u, N_v) \in \mathbb{N}$ are the number of discretizing functions in u and v, respectively, and the functions $y_j(x)$ are polynomials chosen such that u and v and their derivatives satisfy all the boundary conditions. Although the derivation is not reported for sake of conciseness, the polynomials include quadratic, cubic and quartic terms.

The problem can be cast in matrix form introducing the vector of generalized coordinates $\mathbf{q}(t) = \begin{bmatrix}\boldsymbol{\xi}(t)\\ \boldsymbol{\zeta}(t)\end{bmatrix}$ where $\boldsymbol{\xi}(t) = [\xi_1\ \xi_2\ \cdots\ \xi_{N_u}]^\top$ and $\boldsymbol{\zeta}(t) = [\zeta_1\ \zeta_2\ \cdots\ \zeta_{N_v}]^\top$ and $\top$ indicates the transpose. Then, $\boldsymbol{\xi}(t) = \mathbf{B}_u\mathbf{q}$, $\boldsymbol{\zeta}(t) = \mathbf{B}_v\mathbf{q}$, where $\mathbf{B}_u$ and $\mathbf{B}_v$ are Boolean matrices used to extract the appropriate coordinates out of the global generalized vector $\mathbf{q}$. Letting $\boldsymbol{\Phi}_{u1}(x) = \{\sin j\pi x\}$, $\boldsymbol{\Phi}_{u2}(x) = \{jy_j(x)\}$, $(j = 1,\ldots,N_u)$ and $\boldsymbol{\Phi}_v(x) = \{\sin j\pi x\}$, $(j = 1,\ldots,N_v)$, the horizontal and vertical displacement components can be expressed, in

compact form, as

$$u(x,t) = [\boldsymbol{\Phi}_{u1}^{\top}(x)\mathbf{B}_u + \boldsymbol{\Phi}_{u2}^{\top}(x)\mathbf{B}_v]\mathbf{q}(t), \quad v(x,t) = \boldsymbol{\Phi}_v^{\top}(x)\mathbf{B}_v\mathbf{q}(t). \tag{17}$$

First, we introduce the non-dimensional kinetic energy as the summation of the arch and deck kinetic energies; that is,

$$T = T_a + T_d = \frac{1}{2}\int_0^1 \sec\,\theta_n(\dot{u}^2 + \dot{v}^2)\,\mathrm{d}x + \frac{1}{2}\int_0^1 \mu\dot{v}^2\,\mathrm{d}x, \tag{18}$$

where T_a and T_d represent the kinetic energies of the arch and the deck, respectively, and use of $\mathrm{d}s = \cos\theta_n\,\mathrm{d}x$ has been made. The ensuing bridge mass matrix is reported in Appendix. The kinetic energy due to the hanger rods is neglected in Eq. (18) because it is known that the main mass of the bridge is associated with the bridge deck and the arches whereas the hanger rods inertial contribution is, by and large, negligible.

Further, the total potential energy of the bridge is the summation of three contributions, the elastic strain energy of the arch U_a and the deck U_d, respectively, and the potential energy associated with the potential static forces W_c. In dimensionless form, it can be written as

$$U = U_a + U_d - W_c. \tag{19}$$

The arch strain energy is the summation of the bending and the elongation strain energies; that is,

$$U_a = \frac{1}{2}\int_0^1 \kappa_a^2\,\sec\,\theta_n\,\mathrm{d}x + \frac{1}{2}\int_0^1 \alpha\varepsilon_a^2\,\sec\,\theta_n\,\mathrm{d}x. \tag{20}$$

Substituting Eq. (17) into Eqs. (1) and (2), and the resulting expressions into Eq. (20), the arch elastic stiffness matrix is obtained in the form given in Appendix.

Depending on whether the bridge is hinged–hinged or simply supported, the strain energy of the deck is given by the bending energy only or by the summation of the bending and elongation energies, respectively; that is,

$$U_d = \frac{1}{2}\int_0^1 \gamma\kappa_d^2\,\mathrm{d}x \quad \text{or} \quad U_d = \frac{1}{2}\int_0^1 \gamma\kappa_d^2\,\mathrm{d}x + \int_0^1 \Gamma\varepsilon_d^2\,\mathrm{d}x, \tag{21}$$

where $\Gamma = L^2(EA)_d/(EI)_a$ is the deck axial stiffness relative to the arch bending stiffness. In the latter case, it would be necessary to introduce the horizontal displacement of the deck. Henceforth, the first static scheme will only be considered and the resulting deck stiffness matrix is reported in Appendix.

To complete the formulation of the elasto-dynamic problem, the generalized forces are defined according to the virtual work performed by the external forces. Letting δu and δv represent the virtual displacements in the horizontal and vertical directions, the virtual work is expressed as

$$\delta W = \int_0^1 \left[p_1\,\sec\,\theta_n\delta u + \left(p_2\,\sec\,\theta_n + q\right)\delta v\right]\mathrm{d}x + \sum_{j=1}^{N_a}\int_0^1 F_j(t)\delta(x - x_j)\delta v\,\mathrm{d}x, \tag{22}$$

where $\delta(.)$ is the Dirac delta function, N_a is the number of point loads, and x_j is the position at time t of the jth vertical load F_j (see Fig. 1a). Hence, the vector of time-dependent generalized forces is accordingly expressed as

$$\begin{aligned}\mathbf{P}(t) = &\int_0^1 [p_1(x,t)\sec\,\theta_n(\mathbf{B}_u^{\top}\boldsymbol{\Phi}_{u1} + \mathbf{B}_v^{\top}\boldsymbol{\Phi}_{u2}) + (p_2(x,t)\sec\,\theta_n + q(x,t))(\mathbf{B}_v^{\top}\boldsymbol{\Phi}_v)]\,\mathrm{d}x\\ &+ \sum_{j=1}^{N_a}\int_0^1 F_j(t)\mathbf{B}_v^{\top}\boldsymbol{\Phi}_v\delta(x - x_j)\,\mathrm{d}x.\end{aligned} \tag{23}$$

Introducing the system Lagrangian $\mathscr{L} = T - U$, including linear proportional generalized damping forces via the Rayleigh dissipation functional, the Euler–Lagrange's equations yield the equations of motion in compact matrix form as

$$\mathbf{M}\,\ddot{\mathbf{q}}(t) + \mathbf{C}\,\dot{\mathbf{q}}(t) + \mathbf{K}\mathbf{q}(t) = \mathbf{P}(t). \tag{24}$$

3.1. Model validation via finite element analyses: the natural frequencies and mode shapes

The eigenvalue problem is solved to determine the bridge undamped natural frequencies and mode shapes. To this end, the damping and external forces are set to zero yielding the equations of undamped unforced motions, namely, $\mathbf{M}\ddot{\mathbf{q}} + \mathbf{K}\mathbf{q} = \mathbf{0}$.

A preliminary convergence study has been conducted—both on the displacement and internal forces—on the elasto-static response to the gravity forces aimed at assessing the minimum number of discretizing functions leading to an acceptable accuracy. It was found that 20 functions in u and 20 functions in v were sufficient for convergence. Thereafter, letting $\mathbf{q}(t) = \mathbf{U}\exp(\mathrm{i}\omega t)$, the eigenvalue problem $\mathbf{K}\mathbf{U} = \omega^2\mathbf{M}\mathbf{U}$ has been solved.

The proposed DP model and the semi-analytical approach have been validated comparing the obtained natural periods and the associated mode shapes with those obtained via a FE discretization. For this comparison, we considered the geometric and mechanical properties of an existing lower-deck steel truss railway bridge on the Pescara–Bari line along the Adriatic coast in the south-east of Italy. The arch has a parabolic profile with a rise of 17.2 m, a span of 68.60 m; the distance between the hanger rods is 1.225 m. The overall properties are reported in Tables 1 and 2. The considered bridge is representative of typical steel arch bridges with moderate spans. The main horizontal beams are two T-shaped steel beams; further, 4 I-shaped secondary steel beams support the concrete slab with the ballast where the railway tracks are fixed. The arch is made of two II-shaped steel beams and are joined transversely with I-shaped secondary beams at a distance of 9 m.

In the FE calculations performed employing the code SAP2000, the bridge deck is represented by 56 2D FRAME elements, each element is 1.225 m long. Also the arch is made of 56 2D FRAME elements whereas the hanger rods have been modelled as TRUSS elements. Using this FE model, the lowest six natural periods and mode shapes were calculated.

In Table 3, we show the percent differences in the oscillation periods of the lowest six bending modes obtained with the FE model and with the proposed DP model. In Figs. 2 and 3, we show the associated lowest six mode shapes obtained with the DP model and with the FE model, respectively, and again a close agreement can be observed.

The lowest mode is skew-symmetric because such a skew-symmetric mode does not imply an average stretching of the arch centreline which would activate high extensional strain energy. The second mode is a symmetric bending mode with two nodes and the third one is a skew-symmetric mode with three nodes. On the other hand, the fourth mode is a symmetric mode without nodes and is a

Table 1
Properties of the deck

Length (m)	68.6
Area (cm^2)	894
Moment of inertia (cm^4)	8.6×10^5
Weight (kN/m)	7.0
Young modulus (GPa)	205

Table 2
Properties of the arch

Rise (m)	17.2
Area (cm^2)	1204
Moment of inertia (cm^4)	2.75×10^6
Weight (kN/m)	9.4
Young modulus (GPa)	205

Table 3
Comparison of the natural oscillation periods (in s) obtained with the FE model and the parametric model

Model	T_1(s)	T_2(s)	T_3(s)	T_4(s)	T_5(s)	T_6(s)
FE	0.422	0.183	0.098	0.088	0.061	0.043
DP	0.430	0.185	0.099	0.088	0.062	0.043
Δ%	1.86	1.08	1.01	0	1.61	0

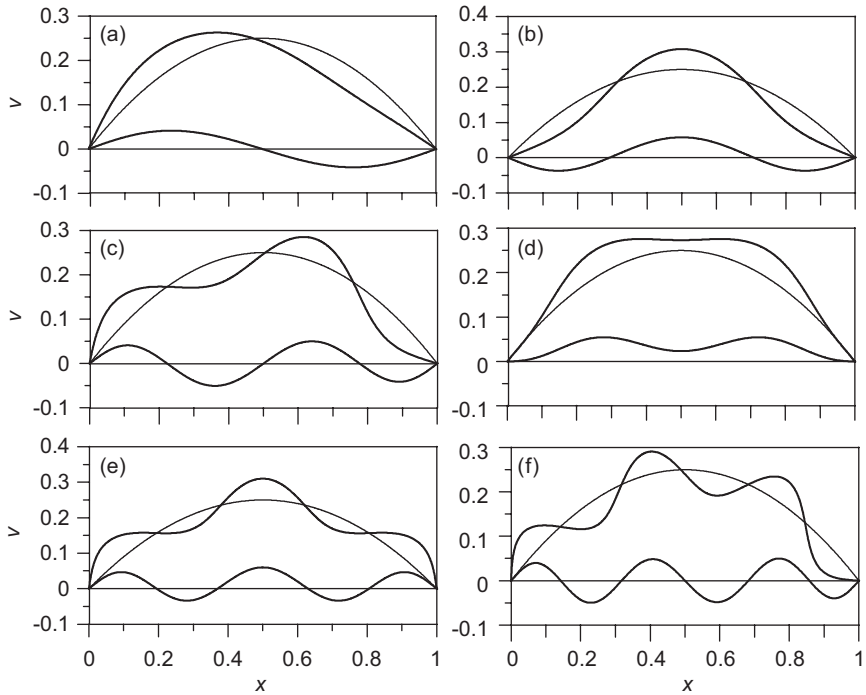

Fig. 2. The lowest six mode shapes of the arch bridge obtained with the distributed-parameter model. The thick (thin) lines denote the modal deformed (undeformed) configurations. (a) = mode 1; (b) = mode 2; (c) = mode 3; (d) = mode 4; (e) = mode 5 and (f) = mode 6.

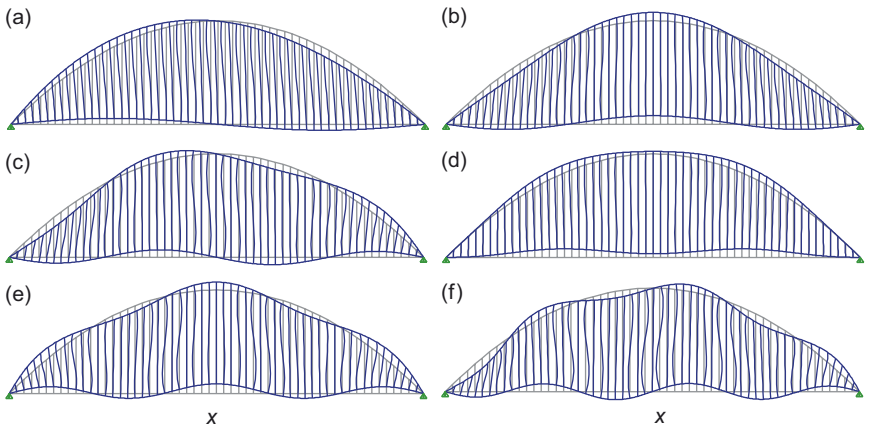

Fig. 3. The lowest six mode shapes of the arch bridge obtained with the FE model. (a) = mode 1; (b) = mode 2; (c) = mode 3; (d) = mode 4; (e) = mode 5 and (f) = mode 6.

bending–stretching mode. The fifth and sixth modes are symmetric and skew-symmetric modes with four and five nodes, respectively. The agreement between the two models is good as expected for both skew-symmetric and symmetric modes since the discrepancy is within a few per cent units, below 2%. The discrepancy is mostly due to the stiffening effect of the FE discretization of the parabolic arch into 56 straight FRAME elements which results into smaller natural periods compared with those obtained with the DP model.

There is an interesting parallel between the sequence of mode shapes in arch bridges and in suspension bridges. In fact, for both bridge schemes, the fundamental mode is a skew-symmetric mode with one node. However, the fundamental symmetric mode with zero nodes, which is the lowest bending mode for the deck by itself and the fundamental stretching mode of the suspension cables appears as the second mode in suspension bridges and as the fourth mode in arch bridges. This mode is higher in arch bridges due to the higher axial modal stiffness of the arch compared with that of the suspension cables.

4. Response to the train passage

In this section, the closed-form solution of the bridge response to the passage of trains with arbitrary load distributions is discussed whereas, in the next section, we elaborate on the resonance conditions.

The solution is determined using the modal superposition approach. With the calculated eigenvectors $\boldsymbol{\psi}_j$, the modal matrix $\boldsymbol{\Psi}$ is constructed collecting them as column vectors. Then, introducing the modal transformation, $\mathbf{q}(t) = \boldsymbol{\Psi}\boldsymbol{\eta}(t)$, where $\boldsymbol{\eta}(t)$ is the vector of normal coordinates, and employing the normalization with respect to the mass matrix, $\boldsymbol{\Psi}^{\top}\mathbf{M}\boldsymbol{\Psi} = \boldsymbol{I}$ ($\boldsymbol{I}$ is the identity matrix), the uncoupled equations of motion in modal space are obtained as

$$\ddot{\boldsymbol{\eta}} + \mathfrak{C}\dot{\boldsymbol{\eta}} + \boldsymbol{\Lambda}\boldsymbol{\eta} = \mathbf{Q}, \tag{25}$$

where $\boldsymbol{\Lambda} = \boldsymbol{\Psi}^{\top}\mathbf{K}\boldsymbol{\Psi} = \mathrm{diag}\{\omega_j^2\}$ is the diagonal matrix of the squared circular frequencies; $\mathfrak{C} = \boldsymbol{\Psi}^{\top}\mathbf{C}\boldsymbol{\Psi} = \mathrm{diag}\{2\nu_j\omega_j\}$, based on the assumption of proportional damping, is the modal damping matrix with ν_j being the jth modal damping ratio; and $\mathbf{Q} = \boldsymbol{\Psi}^{\top}\mathbf{P}$ is the vector of modal forces. The jth equation of motion in the jth normal coordinate is

$$\ddot{\eta}_j(t) + 2\nu_j\omega_j\dot{\eta}_j(t) + \omega_j^2\eta_j(t) = Q_j(t). \tag{26}$$

The main challenge here is to determine closed-form expressions of the train-induced modal forces. To this end, neglecting the elastic and inertial interactions between the train and the bridge, the simplest and most reasonable model of the train (see Fig. 1a) consists in its representation as a number of moving loads with constant speed. When these interactions are accounted for, typically the train compartments are modelled as moving masses connected to the bridge via visco-elastic elements. However, the wide separation between the train frequencies and the bridge frequencies allows to neglect the bridge–train interactions when the interest is mainly on the bridge global responses rather than on the passenger comfort. It is clear that a mechanism that may couple these separated dynamics is due to the track irregularities which, in the worst scenario, could be lateral, vertical, or rotational.

Under the assumption that the tracks are smooth enough to neglect the irregularities, the train loading can be represented by an overall vertical time-dependent force resulting from a series of moving loads with constant speed $V - V$ is the non-dimensional speed obtained from the dimensional speed $\bar{V}$ as $\bar{V}/(\omega_a L)$—which can be expressed as

$$F(x,t) = \sum_{j=1}^{N_a} F_j\delta[x - V(t - t_j^0)][H(t - t_j^0) - H(t - t_j^f)], \tag{27}$$

where $H(.)$ is the Heaviside function; $t_j^0 = \ell_j/V$ is the arriving time of the jth force; $t_j^f = t_j^0 + 1/V$ is the exit time of the jth force; $\ell_j = L_j/L$; L_j indicates the distance between the jth axle and the first axle, and N_a

represents the total number of train axles. The hth component of the generalized force delivered by the train, using Eq. (23) with $p_1 \equiv p_2 \equiv q \equiv 0$, is

$$P_h(t) = \sum_{j=1}^{N_a}\{F_j \int_0^1 \delta[x - V(t-t_j^0)][H(t-t_j^0) - H(t-t_j^f)](\sinh \pi x)\,\mathrm{d}x\}$$
$$= \sum_{j=1}^{N_a}\{F_j \sin(h\pi V(t-t_j^0))[H(t-t_j^0) - H(t-t_j^f)]\}. \tag{28}$$

Hence, the kth modal force generated by the train, using Eq. (28), is expressed as

$$Q_k(t) = \boldsymbol{\psi}_k^{\top}\mathbf{P} = \sum_{h=1}^{N_v}\psi_{hk}P_h(t)$$
$$= \sum_{h=1}^{N_v}\sum_{j=1}^{N_a}\psi_{hk}F_j \sin(\Omega_h(t-t_j^0))[H(t-t_j^0) - H(t-t_j^f)], \tag{29}$$

where ψ_{hk} is the hth component of that part of the kth eigenvector relating to the transverse displacement v (this sub-vector comprises the (N_u+1)th through the (N_u+N_v)th components of $\boldsymbol{\psi}_k$); $\Omega_h = h\pi V$ acts as the forcing circular frequency.

The differential equation in the kth normal coordinate was solved considering the term corresponding to the jth force and hth component [15]. Further, employing the principle of superposition, we obtained the solution corresponding to the first Heaviside function, $H(t-t_j^0)$, representing the forced part of the response. The solution corresponding to natural initial conditions is

$$\eta_{kjh}^0(t) = -\frac{F_j\psi_{hk}}{\omega_k^2}|G_{hk}|\left\{\sin[\Omega_h(t-t_j^0) - \beta_{hk}] + \mathrm{e}^{-\nu_k\omega_k(t-t_j^0)}\left[\sin\beta_{hk}\cos[\tilde{\omega}_k(t-t_j^0)]\right.\right.$$
$$\left.\left. + \frac{1}{\sqrt{1-\nu_k^2}}(\nu_k\sin\beta_{hk} - \alpha_{hk}\cos\beta_{hk})\sin[\tilde{\omega}_k(t-t_j^0)]\right]\right\}H(t-t_j^0), \tag{30}$$

where $\alpha_{hk} = \Omega_h/\omega_k$ and $\tilde{\omega}_k = \omega_k\sqrt{1-\nu_k^2}$ is the damped circular frequency of the kth mode. The dynamic amplification factor and the phase are given by

$$|G_{hk}| = \frac{1}{\sqrt{(1-\alpha_{hk}^2)^2 + (2\nu_k\alpha_{hk})^2}}, \quad \beta_{hk} = \tan^{-1}\left(\frac{2\nu_k\alpha_{hk}}{1-\alpha_{hk}^2}\right). \tag{31}$$

Similarly, the solution corresponding to the second Heaviside function, $-H(t-t_j^f)$, is

$$\eta_{kjh}^f(t) = \frac{F_j\psi_{hk}}{\omega_k^2}|G_{hk}|\left\{\sin[\Omega_h(t-t_j^0) - \beta_{hk}] + \mathrm{e}^{-\nu_k\omega_k(t-t_j^f)}\left[(-1)^h\sin\beta_{hk}\cos[\tilde{\omega}_k(t-t_j^f)]\right.\right.$$
$$\left.\left. + \frac{(-1)^h}{\sqrt{1-\nu_k^2}}(\nu_k\sin\beta_{hk} - \alpha_{hk}\cos\beta_{hk})\sin[\tilde{\omega}_k(t-t_j^f)]\right]\right\}H(t-t_j^f). \tag{32}$$

Therefore, the overall solution in the kth normal coordinate is the summation over j and h of the superposition of the two solutions, (30) and (32); that is,

$$\eta_k(t) = \sum_{h=1}^{N_v}\sum_{j=1}^{N_a} \frac{F_j \psi_{hk}}{\omega_k^2}|G_{hk}| \Bigg\{ -\Bigg[\sin[\Omega_h(t-t_j^0)-\beta_{hk}] + \mathrm{e}^{-v_k\omega_k(t-t_j^0)} \Bigg[\sin\beta_{hk}\cos[\tilde{\omega}_k(t-t_j^0)] + \frac{1}{\sqrt{1-v_k^2}}(v_k\sin\beta_{hk} - \alpha_{hk}\cos\beta_{hk})\sin[\tilde{\omega}_k(t-t_j^0)] \Bigg] \Bigg] H(t-t_j^0) + \Bigg[\sin[\Omega_h(t-t_j^0)-\beta_{hk}] + \mathrm{e}^{-v_k\omega_k(t-t_j^f)} \Bigg[+(-1)^h \sin\beta_{hk}\cos[\tilde{\omega}_k(t-t_j^f)] + \frac{(-1)^h}{\sqrt{1-v_k^2}}(v_k\sin\beta_{hk} - \alpha_{hk}\cos\beta_{hk})\sin[\tilde{\omega}_k(t-t_j^f)] \Bigg] \Bigg] H(t-t_j^f) \Bigg\}. \tag{33}$$

We note that, for times larger than the exit time of the jth force, t_j^f, the forced parts of the responses in η_{kjh}^0 and η_{kjh}^f cancel out and the free oscillatory parts are only left to decay, with a decay rate dictated by the modal damping ratio v_k.

Because $\mathbf{q}(t) = \mathbf{\Psi}\boldsymbol{\eta}(t)$, the displacement field of the arch bridge is expressed as

$$u(x,t) = (\mathbf{\Phi}_{u1}(x)^\top \mathbf{B}_u + \mathbf{\Phi}_{u2}(x)^\top \mathbf{B}_v)\mathbf{\Psi}\boldsymbol{\eta}(t), \quad v(x,t) = \mathbf{\Phi}_v(x)^\top \mathbf{B}_v \mathbf{\Psi}\boldsymbol{\eta}(t). \tag{34}$$

5. Resonance speeds

In this section, the resonances excited by arbitrary trains traversing the bridge are discussed considering the closed-form solution obtained from Eqs. (33) and (34). The main design parameters affecting the dynamic response are also outlined. Thereafter, in the following section, employing the closed-form solution, we document the main results on the investigations into the bridge responses to the passage of three representative European high-speed trains, namely the French TGV, the Italian ETR 500, and the German ICE.

Preliminarily, it is worth discussing in a general fashion the resonance conditions induced by the train transit so that the responses reported in the next section can be interpreted within a sound theoretical framework. This can be directly achieved considering the response in the kth mode during the forced phase, Eq. (30), when $t \in [t_j^0, t_j^f]$, and determine the conditions when this response exhibits a maximum. In particular, the maximum dynamic amplification factor is attained when $|G_{hk}|$ is maximum. This occurs when $\alpha_{hk} \approx 1$, that is, $\Omega_h \approx \omega_k$.

Moreover, let us consider the pth and qth terms, due to the pth and qth loads, contributing to η_k, namely, $\sin(\Omega_h(t-t_p^0)-\beta_{hk})$ and $\sin(\Omega_h(t-t_q^0)-\beta_{hk})$. The sum of these terms is maximum when the relative phase is $2n\pi$, $n \in \mathbb{N}$. The relative phase depends on the time lag between the forces multiplied by Ω_h, that is, $\Omega_h(t_q^0 - t_p^0)$. Since $t_j^0 = \ell_j/V$, it follows $\Omega_h(t_q^0 - t_p^0) = (\ell_q - \ell_p)\Omega_h/V$. Hence, the maximum is achieved when $(\ell_q - \ell_p)\omega_k/V \approx 2n\pi$; consequently, the non-dimensional and dimensional speeds causing the resonance of the kth mode are obtained as

$$V_k = (\ell_q - \ell_p)\frac{\omega_k}{2n\pi}, \quad \bar{V}_k = (L_q - L_p)\frac{f_k}{n} \tag{35}$$

with $(L_q - L_p) < L, n \in \mathbb{N}$, and $f_k = \omega_a(\omega_k/(2\pi))$ is the dimensional frequency (in Hz) of the kth mode. This condition implies that, if p and q relate to the loads carried by the front and rear axles of the same train compartment, then denoting with $L_c = L_q - L_p$ the characteristic length of the compartment, the resonance speed is $\bar{V}_k = (L_c f_k)/n$. Hence, it turns out that L_c is the leading parameter in the resonance condition.

Table 4
Resonance speeds (in km/h) of the lowest four modes for the TGV, ETR, ICE trains traversing the considered steel arch bridge

Train	Mode 1	Mode 2	Mode 3	Mode 4
TGV ($L_c = 18.7$ m)	150	348	645	682
ETR ($L_c = 19$ m)	153	353	656	693
ICE ($L_c = 19.5$ m)	157	363	673	711

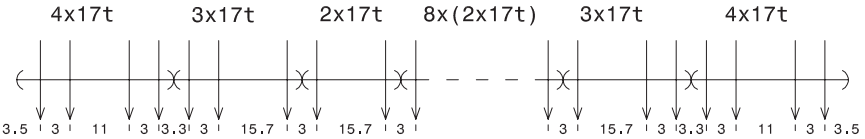

Fig. 4. Scheme of the TGV forces according to the design codes (design speed $\bar{V} = 350$ km/h); t denotes tons and the distances are in meters.

In Table 4, the resonance speeds of the lowest four modes of the considered lower-deck steel arch bridge are calculated and reported for the TGV, ETR 500, and ICE trains. The characteristic lengths are obtained from the train load distributions shown in Figs. 4, 8 and 11.

A weaker resonance, as previously discussed, is excited when only $|G_{hk}|$ is maximum although the phasing between the contributions generated by the loads in the kth mode is not an integer multiple of 2π. In such a circumstance, the resonance occurs when $\alpha_{hk} \approx 1$. Consequently, the non-dimensional and dimensional resonance speeds become, respectively,

$$V_k = \frac{\omega_k}{h\pi}, \quad \bar{V}_k = 2L\frac{f_k}{h}, \tag{36}$$

where h indicates the component number of the kth sub-eigenvector relating to the vertical displacement. It is worth observing that this resonance corresponds to the resonance condition under one single travelling load and depends on the length of the bridge and the frequency of the excited mode [2, 4], hence, it does not account for the actual distribution of the loads carried by a specific train. To determine h in Eq. (36), we consider the vector ψ_{hk} to identify which h is such to determine the highest contribution of the corresponding trial function $\sin h\pi x$ in the vertical displacement associated with the kth mode shape. In the considered bridge problem, observing the mode shapes, it is $h = 2$ for $k = 1$, then the speed of the train that would excite at resonance the lowest mode is $\bar{V} \simeq 551$ km/h.

Shen-Haw and Hung-Ta [12], while studying the dynamic response of different steel arch bridges, determined two criteria to predict the train-induced bridge resonances and validated them employing FE analyses. According to the first criterion, when $n\bar{V}/L_c$ is close to the lowest bridge natural frequencies, a resonance is excited, where n is a positive integer. The second criterion is that the resonance of the lowest mode is excited when the train velocity is higher than $Lf_2/2$, where L is the bridge length and f_2 is the bridge natural frequency of the skew-symmetric mode. These conditions are in agreement with the conditions here discussed based on the closed-form solution.

It is worth observing that the obtained resonance conditions are valid also for general simply supported straight bridges. The difference between the two structural schemes is that for simply supported bridges, the modes belong to a complete sequence of purely bending modes whereas, in arch bridges, the modes are bending and bending–stretching modes. In particular, the lowest mode is a bending skew-symmetric mode with one node while the lowest hybrid bending–stretching mode without nodes manifests itself in the fourth mode. Therefore, the responses of the two types of bridges to the passage of trains are expected to be quite different.

6. Response analysis of a steel arch bridge traversed by European high-speed trains

In this section, the prominent features of the responses of the considered lower-deck steel arch bridge to the passage of three European high-speed trains are illustrated.

In Fig. 4, the shown loading scheme of the TGV train used for bridge design purposes is employed for calculating the dynamic response. In Fig. 5, variation of the maximum bridge deflection at $x = 3/4$ in the time interval $[0, t_u]$ is shown when the train speed is varied between 100 and 200 km/h. The ensuing curve is a speed-response curve (as a frequency-response curve) with the train speed being the control parameter. Here and henceforth, t_u indicates the time instant when the train leaves the bridge. Considering the length of the intermediate compartments, the characteristic length of the TGV train is $L_c = 18.7$ m, hence, the calculated lowest resonance speed is about 150 km/h, in agreement with the observed first resonance peak in Fig. 5. However, another peak in the lowest skew-symmetric mode is observed when the speed is about 158 km/h. This implies that there is another characteristic length of about 19.7 m which is likely related to the other compartments along the train as it can be inferred from Fig. 4.

In Fig. 6, we show the lowest six modal forces, in the time interval $[0, t_u]$, due to the transit of the TGV on the bridge at the design speed of 350 km/h. The modal forces are significant for the skew-symmetric modes, namely the first, third, and sixth modes (see Fig. 2) and are of the same order of magnitude whereas they are negligible for the symmetric modes, namely, the second, fourth and fifth modes. This implies that the resonant responses would be observed in the skew-symmetric modes only.

In Fig. 7, the time histories of the deflection and acceleration of the bridge deck at $x = 3/4$ and $1/2$, respectively, are shown. The transit speed, corresponding to the design speed, is close to the resonance speed of the lowest symmetric mode (mode 2 in Table 4); however, this resonance is not developed due to the fact that the projection of the train forces onto this symmetric mode is negligible (see Fig. 6). As a result, the response

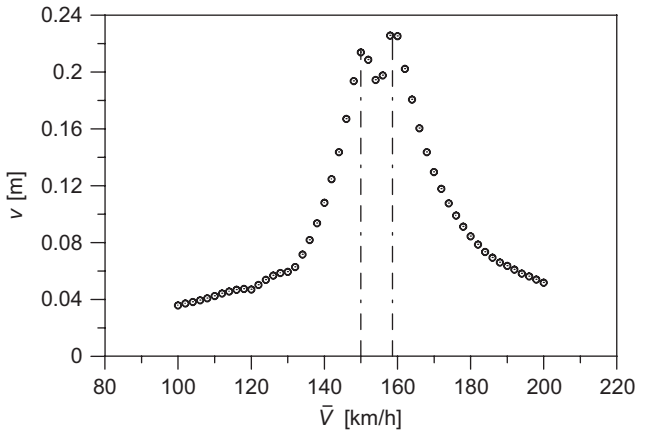

Fig. 5. Variation of the deflection at $x = 3/4$ with the TGV train speed: Resonance of the lowest mode.

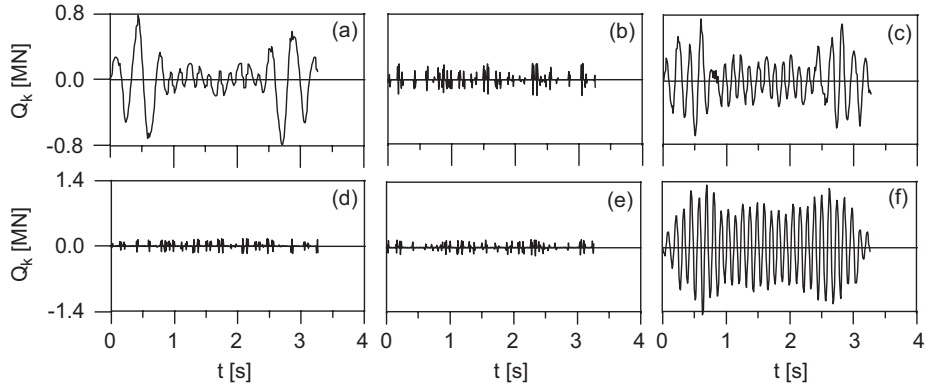

Fig. 6. Transit of the TGV train at the design speed ($\bar{V} = 350$ km/h): lowest six modal forces in MN (10^6 N). (a) = mode 1; (b) = mode 2; (c) = mode 3; (d) = mode 4; (e) = mode 5 and (f) = mode 6.

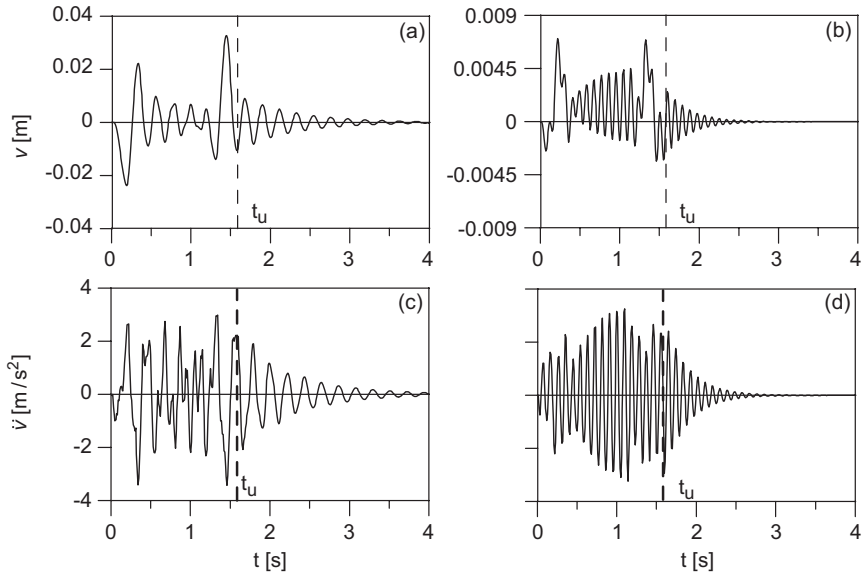

Fig. 7. Transit of the TGV train at the design speed: time histories of the deck deflection at (a) $x = 3/4$ and (b) $x = 1/2$ and the acceleration at (c) $x = 3/4$ and (d) $x = 1/2$.

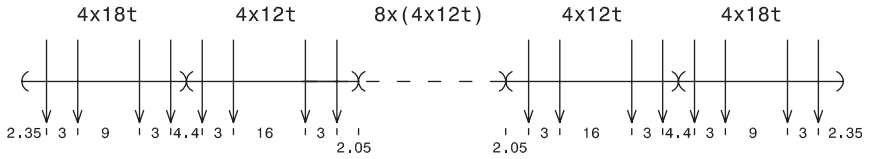

Fig. 8. Scheme of the ETR forces according to the codes (design speed $\bar{V} = 300\,\mathrm{km/h}$).

peak is higher at $x = 3/4$ because the skew-symmetric modal forces are order-of-magnitude higher than the symmetric forces. The peak deflection is attained a few fractions of second before the train has completely passed the bridge. Past t_u, the response is that of a damped unforced system as expected. Further, the differences in the frequencies of the observed motions at $x = 1/2$ and $3/4$ are due to the fact that the mid-span is a node of vibration of the skew-symmetric modes. Therefore, at the mid-span section, the leading frequency is that associated with the second mode (the lowest symmetric mode), whereas the frequencies associated with the skew-symmetric modes are not observed. On the other hand, at $x = 3/4$ we note the contribution from the low-frequency first mode which exhibits higher amplitudes than that arising from the second mode due to the mentioned differences in magnitude of the modal forces (see Fig. 6). As to the time histories of the accelerations at $x = 3/4$ and $1/2$ (Fig. 7c,d), the order-of-magnitude at the mid-span and at three-quarter span is the same and the higher frequency of the lowest symmetric mode in Fig. 7d is evident.

In Fig. 8, the loading scheme of the Italian ETR 500 train, according to the design codes, is shown. This train is supposed to reach a maximum speed of 300 km/h. In Fig. 9, we show the time histories of the lowest six modal forces, in the time interval $[0, t_u]$, excited by the transit of the ETR 500 on the bridge at its design speed. The pattern of these forces is similar to that of the TGV forces, namely, they are significant for the skew-symmetric modes whereas they are practically negligible for the symmetric modes. In Fig. 10, the time histories of the deflections and accelerations are shown at $x = 3/4$ and $1/2$, respectively. The peak deflection at $x = 3/4$ is slightly smaller than that caused by the TGV train whereas the peak acceleration is nearly halved.

Finally, in Fig. 11, the loading scheme of the German ICE train (maximum design speed of 250 km/h) is shown. Fig. 12 portrays the time histories of the lowest six modal forces due to the transit of the ICE train at the design speed of 250 km/h. As expected, the pattern of these forces is again similar to the previously discussed train-induced modal forces. However, here we note that the modal forces associated with the second

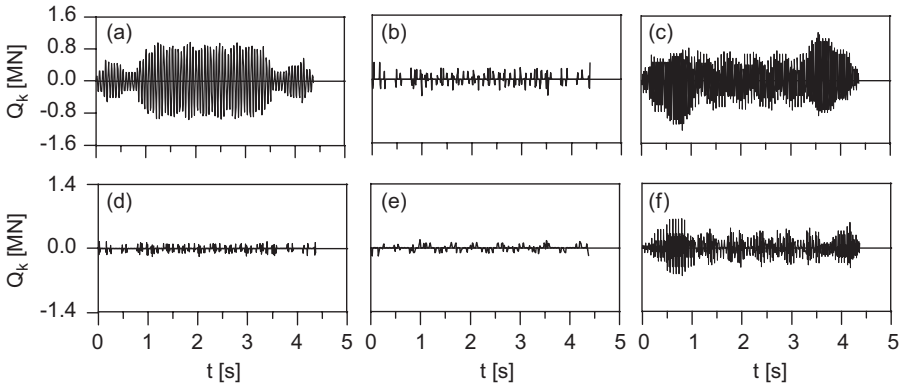

Fig. 9. Transit of the ETR train at the design speed ($\bar{V} = 300\,\mathrm{km/h}$): lowest six modal forces. (a) = mode 1; (b) = mode 2; (c) = mode 3; (d) = mode 4; (e) = mode 5 and (f) = mode 6.

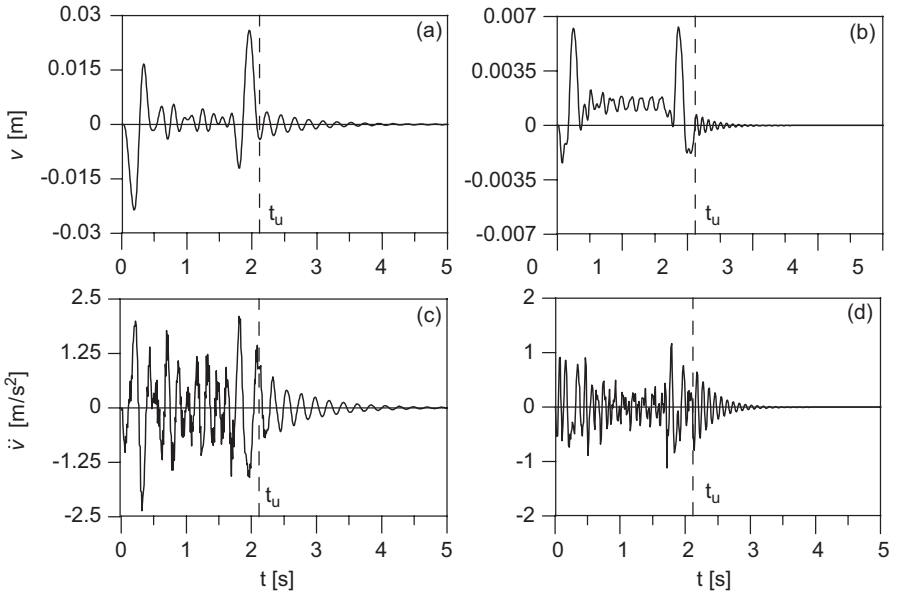

Fig. 10. Transit of the ETR train at the design speed: time histories of the deck deflection at (a) $x = 3/4$ and (b) $x = 1/2$ and the acceleration at (c) $x = 3/4$ and (d) $x = 1/2$.

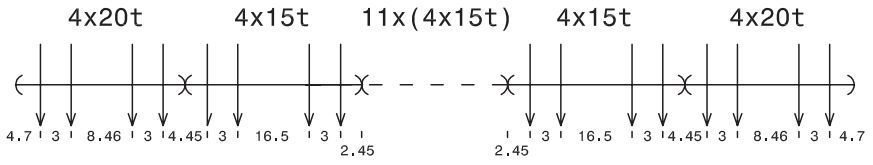

Fig. 11. Scheme of the ICE forces according to the codes (design speed $\bar{V} = 250\,\mathrm{km/h}$).

and third skew-symmetric modes are higher than the modal force associated with the lowest skew-symmetric mode. In Fig. 13, the ensuing time histories of the deflections and accelerations at $x = 3/4$ and $1/2$, respectively, are shown. In this case, the peak values are comparable with those of the response excited by the ETR 500.

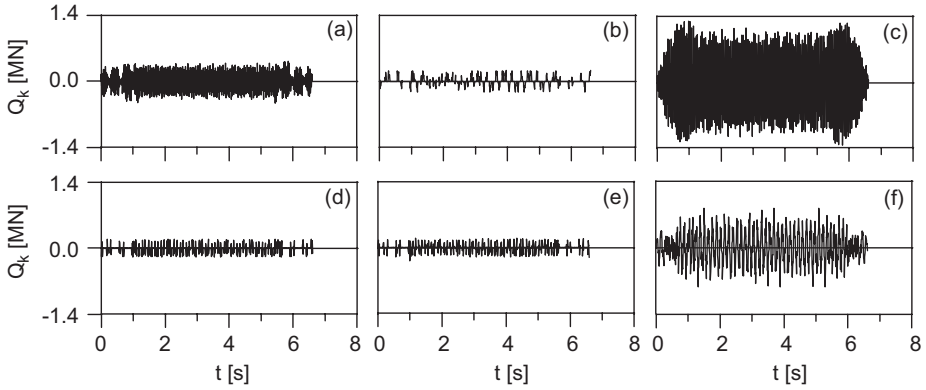

Fig. 12. Transit of the ICE train at the design speed ($\bar{V} = 250$ km/h): lowest six modal forces. (a) = mode 1; (b) = mode 2; (c) = mode 3; (d) = mode 4; (e) = mode 5 and (f) = mode 6.

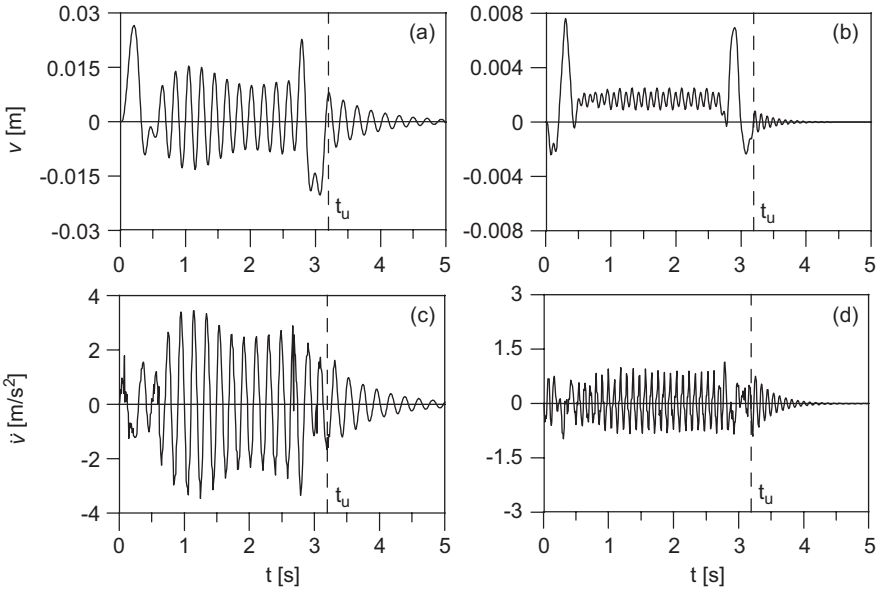

Fig. 13. Transit of the ICE train at the design speed: time histories of the deck deflection at (a) $x = 3/4$ and (b) $x = 1/2$ and the acceleration at (c) $x = 3/4$ and (d) $x = 1/2$.

7. Conclusions

A distributed-parameter (DP) model of arch bridges subject to general excitations is proposed; in particular, a closed-form representation of the actual load distribution of running trains is considered using unit step functions. The governing equations of motion, ensuing from the balance of linear and angular momentum, are two coupled partial-differential equations in the horizontal and vertical displacement components. Due to the non-uniform geometric curvature of the arch profile, the equations of motion exhibit variable coefficients. A semi-analytical solution scheme based on Ritz's method is conveniently employed to calculate the bridge natural frequencies and mode shapes. The DP model and the semi-analytical solution approach are validated comparing the calculated linear vibration properties with those obtained via a finite element (FE) code and a close agreement has been shown.

A closed-form solution of the arch bridge dynamic responses excited by the transit of high-speed trains is found neglecting the elastic and inertial interactions between the train and the bridge and using

the modal superposition approach. The transit of trains mostly generates skew-symmetric forces, thus exciting prevalently skew-symmetric vibrations, greatly amplified around the resonances of the bending modes.

The solution obtained in the time domain allows to determine the resonance speeds of the bridge modes in closed form. These resonance speeds are numerically verified employing the Ritz's computational scheme applied to an existing lower-deck steel arch bridge with a parabolic arch profile and are in agreement with previous studies mostly conducted using FE schemes. The closed-form solution is effective for investigating the leading properties of the dynamic responses to different trains and transit speeds and different arch bridge geometries and design parameters. In this paper, three representative European high-speed trains are considered, namely, the French TGV, the Italian ETR 500, and the German ICE. These trains are assumed to traverse the considered lower-deck steel arch bridge at their design speeds. In all cases, it is found that, although the speeds are close to the resonance speeds of the lowest symmetric mode of the bridge, because the associated modal forces are order-of-magnitude smaller than those associated with skew-symmetric modes, the ensuing vibrations are prevalently skew-symmetric. Further, it is observed that the peak deflections are attained a few fractions of second after the train has entered the bridge and slightly before the train has completely passed the bridge.

The proposed closed-form solution and resonance conditions turn out to be particularly useful for the design of tuned-mass dampers or other vibration mitigation strategies which are the primary focus of a companion manuscript.

Acknowledgments

This work was partially supported by the Italian Ministry of Education, University and Scientific Research under the FY 2003-2004 PRIN Grant "Analysis, experiment, identification, control of models, prototypes and full-scale structures".

Appendix. The mass and stiffness matrices

The mass matrix is given by

$$\mathbf{M} = \int_0^1 [\sec\theta_n(\mathbf{B}_u^\top \boldsymbol{\Phi}_{u1}\boldsymbol{\Phi}_{u1}^\top \mathbf{B}_u + \mathbf{B}_v^\top \boldsymbol{\Phi}_{u2}\boldsymbol{\Phi}_{u2}^\top \mathbf{B}_v) + (\sec\theta_n + \mu)(\mathbf{B}_v^\top \boldsymbol{\Phi}_v \boldsymbol{\Phi}_v^\top \mathbf{B}_v)]\,\mathrm{d}x. \tag{37}$$

The arch and deck stiffness matrices are, respectively, in the forms

$$\begin{aligned}\mathbf{K}_a = \int_0^1 \Bigg\{ &\left[-\frac{1}{2}(\mathbf{B}_u^\top \boldsymbol{\Phi}_{u1}' + \mathbf{B}_v^\top \boldsymbol{\Phi}_{u2}')\sin 2\theta_n + \mathbf{B}_v^\top \boldsymbol{\Phi}_v' \cos^2\theta_n\right]' \\ &\times \left[-\frac{1}{2}(\boldsymbol{\Phi}_{u1}'^\top \mathbf{B}_u + \boldsymbol{\Phi}_{u2}'^\top \mathbf{B}_v)\sin 2\theta_n + \boldsymbol{\Phi}_v'^\top \mathbf{B}_v \cos^2\theta_n\right]' \cos\theta_n\,\mathrm{d}x \\ &+ \int_0^1 \left[(\mathbf{B}_u^\top \boldsymbol{\Phi}_{u1}' + \mathbf{B}_v^\top \boldsymbol{\Phi}_{u2}')\cos^2\theta_n + \frac{1}{2}\mathbf{B}_v^\top \boldsymbol{\Phi}_v' \sin 2\theta_n\right]\alpha \\ &\times \left[(\boldsymbol{\Phi}_{u1}'^\top \mathbf{B}_u + \boldsymbol{\Phi}_{u2}'^\top \mathbf{B}_v)\cos^2\theta_n + \frac{1}{2}\boldsymbol{\Phi}_v'^\top \mathbf{B}_v \sin 2\theta_n\right]\Bigg\} \sec\theta_n\,\mathrm{d}x,\end{aligned} \tag{38}$$

$$\mathbf{K}_d = \mathbf{B}_v^\top \left(\int_0^1 \boldsymbol{\Phi}_v'' \gamma \boldsymbol{\Phi}_v''^\top \,\mathrm{d}x\right)\mathbf{B}_v. \tag{39}$$

The global stiffness matrix of the bridge is $\mathbf{K} = \mathbf{K}_a + \mathbf{K}_d$.

References

[1] L. Bolotin, *The Dynamic Stability of Elastic Systems*, Holden-Day, San Francisco, 1964.
[2] L. Fryba, *Vibration of Solids and Structures Under Moving Loads*, Noordhoff International Publishing, The Netherlands, 1972.
[3] J.S. Wu, L.K. Chiang, Dynamic analysis of an arch due to a moving load, *Journal of Sound and Vibration* 269 (2004) 511–534.
[4] W. Lacarbonara, R.R. Soper, A.H. Nayfeh, D.T. Mook, Resonances of stiff-span bridges under a moving load, *AIAA/ASME/ASCE/AHS/ASC Structures, Structural Dynamics, and Materials Conference*, American Institute of Aeronautics and Astronautics, Paper No. AIAA-1997-1099, FL, 1997, pp. 387–394.
[5] F.T.K. Au, J.J. Wang, Y.K. Cheung, Impact study of cable-stayed bridge under railway traffic using various models, *Journal of Sound and Vibration* 240 (2001) 447–465.
[6] Y.B. Yang, J.D. Yau, L.C. Hsu, Vibration of simple beams due to trains moving at high speeds, *Engineering Structures* 19 (1997) 936–944.
[7] M. Klasztorny, Vertical vibrations of a multi-span beam steel bridge induced by a superfast passenger train, *Structural Engineering and Mechanics* 23 (2001) 1597–1606.
[8] H. Xia, N. Zhang, Dynamic analysis of railway bridge under high-speed trains, *Computers & Structures* 23 (2005) 1891–1901.
[9] H. Xia, N. Zhang, R. Gao, Experimental analysis of railway bridge under high-speed trains, *Journal of Sound and Vibration* 282 (2005) 517–528.
[10] J.W. Kwark, E.S. Choi, Y.J. Kim, B.S. Kim, S.I. Kim, Dynamic behaviour of two-span continuous concrete bridges under moving high-speed train, *Computers & Structures* 82 (2004) 463–474.
[11] T. Yanagi, A. Nakajima, L. Saiki, Two-dimensional elasto-plastic behaviour of deck type steel arch bridge and its modeling, *Journal of Structural Engineering* 49A (2003) 543–552.
[12] J. Shen-Haw, L. Hung-Ta, Numerical investigation of a steel arch bridge and interaction with high-speed trains, *Engineering Structures* 25 (2005) 241–250.
[13] J.M.W. Brownjohn, Vibration characteristics of a suspension footbridge, *Journal of Sound and Vibration* 202 (1997) 29–46.
[14] J.M.W. Brownjohn, Observations on non-linear dynamic characteristics of suspension bridges, *Earthquake Engineering and Structural Dynamics* 23 (1994) 1351–1367.
[15] L. Meirovitch, *Computational Methods in Structural Dynamics*, Sijthoff and Noordhoff Int., Alphen a/d Rijin, 1996.